

A Fault-Tolerant Integrated Vehicle Stability Control Using Adaptive Control Allocation

Ozan Temiz¹, Melih Cakmakci¹, and Yildiray Yildiz¹

Abstract—The focus of this paper is an integrated, fault-tolerant vehicle supervisory control algorithm for the overall stability of ground vehicles. Vehicle control systems contain many sensors and actuators that can communicate with each other over communication networks. The proposed supervisory control scheme is composed of a high-level controller that creates a virtual control input vector and a low-level control allocator that distributes the virtual control effort among redundant actuators. Virtual control input incorporates the required traction force, yaw, pitch, and roll moment corrections, and the lateral force correction to ensure stability while following a maneuvering reference initiated by the driver. Based on the virtual control input vector, the allocation module determines front steering angle correction, rear steering angle, traction forces at each tire, and active suspension forces. The proposed control framework distinguishes itself from earlier results in the literature by its ability to adapt to failures and uncertainties by updating its parameters online, without the need for fault identification. The control structure is validated in the simulation environment using a fourteen degree of freedom nonlinear vehicle model. Our results demonstrate that the proposed approach ensures that the vehicle follows references created by the driver despite the loss of actuator effectiveness up to 30% higher longitudinal maneuver velocity and approximately 35% lower roll and pitch angles during steering with representative driving scenarios.

Index Terms—Control Allocation, Vehicle Control, Fault-Tolerance

I. INTRODUCTION

Over the past two decades, there have been many advancements in the automotive field with the increased cooperation among vehicle subsystems that are traditionally designed separately. Vehicle communication networks, low-cost sensors, and dependable mechatronic actuators play an essential role in this new trend, enabling engineers to design an automobile as a single mechatronic system. This new cooperative approach generates redundancies in control problems, as reported in [1]–[3]. Availability of various actuators, together with the cross-coupling between lateral and rotational dynamics, has led to the integrated vehicle control algorithms such as those proposed in [4]–[14]. These algorithms can exploit coupled dynamics, producing better performance by adjusting actuator inputs accordingly.

Actuation redundancy in ground vehicles can be observed, for example, in yaw rate control (vehicle’s rotation about the z-axis). Yaw rate can be regulated using both steering and traction systems: A vehicle can regulate its yaw rate by altering the amount of longitudinal traction forces at different wheels,

thanks to in-wheel electric motors. Another way of altering the yaw rate is the steering input. While only front-wheel steering was available and the amount of steering was mechanically constrained in the past, steer by wire and four-wheel-steering technology recently became feasible and affordable with the introduction of dependable, low-cost actuators and enabling control strategies [15] and [16]. Such developments in the industry introduced redundancy and created new opportunities for control researchers.

An important challenge to utilize these control redundancies is to find precise approaches that can be implemented for a wide range of vehicle control problems. These approaches need to overcome the computational complexity due to the increased number of performance requirements and constraints originating from subsystem controller design problems. “Control allocation” [9] can be defined as a systematic way of distributing the total control effort among different actuators. Control allocation is widely used in flight control to determine the control surface deflections based on a total virtual control input generated by a high-level controller [17]–[19]. Schemes involving control allocators are usually composed of three successive steps: In the first step, a virtual control input (for example, the required total force or moment vector to move an object) is determined by a high-level controller such that the overall control objective is met. In the second step, the control allocation receives this virtual control input and determines individual actuator commands based on a certain allocation policy. Finally, as the last step, actuator controllers ensure the realization of these commands. Block diagrams of closed-loop control architectures with and without a control allocator are presented in Fig. 1 as parts (a) and (b), respectively.

There are several novel controller design ideas proposed in the automotive control literature that successfully manage actuator redundancy. Control allocation for torque vectoring is used in [20] considering power management, traction control, actuator limits, and fault-cases. In [21], a fixed point control allocation algorithm distributes the slip among tires with low computational effort. In [22], a fault-tolerant control architecture is proposed, which can switch between two optimal control allocation schemes. In [23], a control allocation algorithm decides the required torques by taking the controller area network (CAN) communication into consideration. In [24], an adaptive control allocation is used for energy-efficient path following using regenerative braking in electric ground vehicles. In [25], another adaptive control allocation application is presented, where the approach given in [26] is used.

In this paper, an integrated vehicle controller incorporating an adaptive control allocator is proposed. In order to ensure

¹Ozan Temiz, Melih Cakmakci (corr. author) and Yildiray Yildiz are with the Department of Mechanical Engineering, Bilkent University, Ankara 06800, Turkey. ozan.temiz.93@gmail.com, [melihc, yyildiz]@bilkent.edu.tr

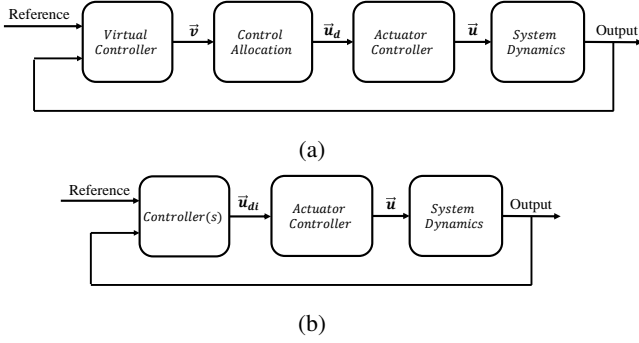
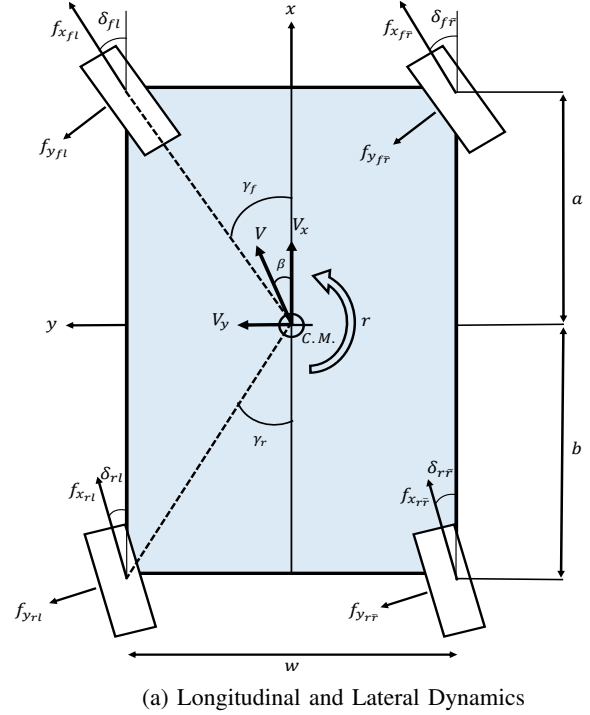


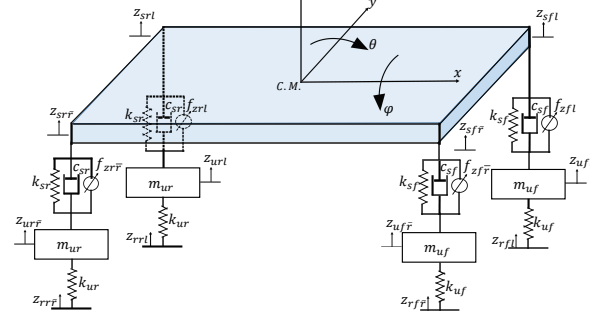
Fig. 1: (a) Block diagram of a control system with a control allocator, where \vec{v} is the virtual control input vector, \vec{u}_d is the desired actuator response vector and \vec{u} is the actuator commands vector to achieve the desired response, and (b) block diagram of a control system where the controller produces individual actuator commands, \vec{u}_{di} , directly.

that the vehicle follows the driver's intentions, first, a high-level controller generates the virtual control input vector. This vector consists of the desired traction force, yaw, pitch and roll moment, and the required lateral force correction based on the steering and pedal inputs from the driver. Then, the control allocation algorithm generates the front steering angle correction, rear steering angle, traction forces, and the active suspension forces at each wheel. The desired moments and the traction forces are delivered such that the vehicle rotates and accelerates as needed while desired yaw and pitch moments increase the normal forces, when necessary, at individual wheels to provide both stability and driver comfort. Required lateral force correction ensures that the side-slip angle is in the stable region while following the yaw reference signal. This paper is a continuation of our work given in [27] and [28]. In [27], a simpler two-track vehicle model was used for traction control only. In [28], our earlier work was extended with passive suspension dynamics, and the traction control performance in the presence of communication delay in actuators and sensors was studied.

The contributions of this study can be listed as follows: (1) A detailed control-oriented nonlinear vehicle model is developed that is suitable for wheel-based traction, steering, and suspension control studies with necessary longitudinal, lateral, and vertical motion fidelity. This model is also validated against a multi-body dynamics based commercial software [29]. (2) Inspired from [30], [31] and [32], a controller framework involving a fault-tolerant control allocation algorithm is developed, which is capable of controlling the longitudinal, lateral and vertical vehicle dynamics in an integrated manner. To achieve this, the control allocation presented in [30] and [31] had to be extended to handle the class of systems that have time-varying control input matrix dynamics. To the best of our knowledge, this study is the first of its kind in its attempt to outline a method to develop an integrated vehicle stability controller that utilizes vectoring, steering, and suspension control systems at the same time, in the presence of uncertainties and faults.



(a) Longitudinal and Lateral Dynamics



(b) Vertical Dynamics

Fig. 2: Vehicle Dynamic Model

The remainder of this paper is structured as follows. In Section II, the 14 degrees of freedom vehicle model is presented. In Section III, the overall structure of the integrated vehicle controller, including the control allocation, is explained. Then, the proposed controller is validated via simulation studies in section IV. Lastly, in Section V, a summary is given.

II. MATHEMATICAL MODEL

In this section, the development of a 14 degree of freedom vehicle model is discussed. This model includes all three translation and rotation motions of the vehicle body in the three-dimensional space, together with the elevation and the (z -axis) rotation of each wheel. In order to complete this model, longitudinal, lateral, and vertical motions of the vehicle mass, and each wheel need to be considered (see Fig. 2). Most models in the literature contain vehicle translational and rotational motions in one or two directions separately for controller development. However, the model developed in this section considers the vehicle's motion in three directions, including

TABLE I: List of Used Vehicle Parameters

h	Height of the vehicle Center of Gravity (CoG)	0.375 m
a	Length between the front axle and the CoG	1.125 m
b	Length between the rear axle and the CoG	1.375 m
w	Width of the wheelbase	1.6 m
m	Vehicle mass	1300 kg
I_x	Veh. moment of inertia about x - axis	250 kgm^2
I_y	Veh. moment of inertia about y - axis	1000 kgm^2
I_z	Veh. moment of inertia about z - axis	1300 kgm^2
I_w	Wheel moment of inertia	2.7 kgm^2
R_w	Wheel radius	0.33 m
m_{uf}	Front unsprung mass	30 kg
m_{ur}	Rear unsprung mass	30 kg
k_{uf}	Front unsprung spring coefficient	$2 \cdot 10^5$ N/m
k_{ur}	Rear unsprung spring coefficient	$2 \cdot 10^5$ N/m
k_{sf}	Front sprung spring coefficient	$21 \cdot 10^3$ N/m
c_{sf}	Front sprung damping coefficient	1000 Ns/m
k_{sr}	Rear sprung spring coefficient	$21 \cdot 10^3$ N/m
c_{sr}	Rear sprung damping coefficient	1500 Ns/m
A_f	Frontal area of the vehicle	2.2 m^2
C_d	Drag coefficient of the vehicle	0.3

detailed axis interactions. This model helps to achieve the objective of developing controllers for steering, and suspension systems concurrently. The list of parameters used in the model is given in Table I.

A. Longitudinal and Lateral Dynamics

The dynamic equations describing the longitudinal and lateral motions of the vehicle body can be developed by using the variables and vehicle geometry presented in Fig. 2a. Vehicle motion can be described using a coordinate system, xyz , which is fixed to the center of mass of the vehicle, as shown in Fig. 2b.

The total forces in the x -direction, F_x , and in the y -direction, F_y , are calculated as the sum of forces on each tire as

$$F_x = \sum_{i=\{f,r\}} \sum_{j=\{l,\bar{r}\}} F_{xij} \quad (1)$$

$$F_y = \sum_{i=\{f,r\}} \sum_{j=\{l,\bar{r}\}} F_{yij}, \quad (2)$$

where f , r , l and \bar{r} indicate front, rear, left and right wheel locations, respectively. For example, F_{xfl} represents the longitudinal traction force acting on the front left tire. Since each wheel is steerable, these forces can be calculated in terms of the force acting on each tire and the individual steering angles as

$$\begin{aligned} F_{xfl} &= f_{xfl} \cos \delta_{fl} - f_{yfl} \sin \delta_{fl} \\ F_{yfl} &= f_{yfl} \cos \delta_{fl} + f_{xfl} \sin \delta_{fl} \\ F_{xf\bar{r}} &= f_{xf\bar{r}} \cos \delta_{f\bar{r}} - f_{yf\bar{r}} \sin \delta_{f\bar{r}} \\ F_{yf\bar{r}} &= f_{yf\bar{r}} \cos \delta_{f\bar{r}} + f_{xf\bar{r}} \sin \delta_{f\bar{r}} \\ F_{xrl} &= f_{xrl} \cos \delta_{rl} - f_{yrl} \sin \delta_{rl} \\ F_{yrl} &= f_{yrl} \cos \delta_{rl} + f_{xrl} \sin \delta_{rl} \\ F_{xr\bar{r}} &= f_{xr\bar{r}} \cos \delta_{r\bar{r}} - f_{yr\bar{r}} \sin \delta_{r\bar{r}} \\ F_{yr\bar{r}} &= f_{yr\bar{r}} \cos \delta_{r\bar{r}} + f_{xr\bar{r}} \sin \delta_{r\bar{r}}, \end{aligned} \quad (3)$$

where f_{xij} and f_{yij} are the longitudinal and the lateral forces, at tire ij , $i \in \{f, r\}$, $j \in \{l, \bar{r}\}$. The longitudinal acceleration

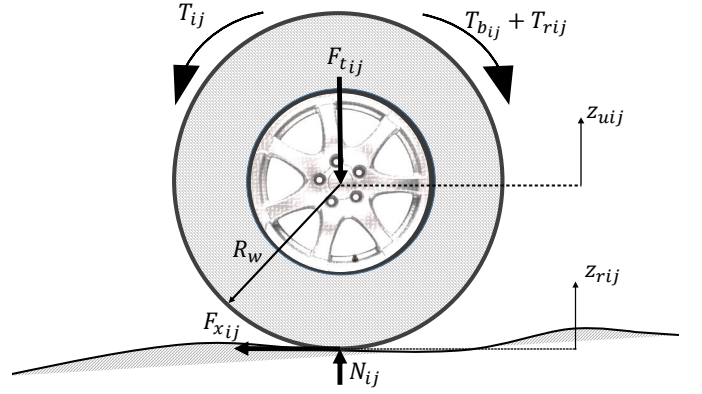


Fig. 3: Tire Dynamics

of the vehicle can be calculated as

$$a_x = \frac{1}{m} [F_x - \frac{1}{2} C_d \rho A_f V_{ar}^2 - mg \sin(Q)], \quad (4)$$

where C_d is the drag coefficient, ρ is the air density, A_f is the frontal area of the vehicle, V_{ar} is the relative velocity between the displaced air and the vehicle, Q is the road slope, and m is the mass of the vehicle. Similarly, lateral acceleration, a_y , can be calculated as

$$a_y = \frac{1}{m} F_y. \quad (5)$$

It is important to note that the coordinate system $[x, y, z]$ moves and rotates with the vehicle. Therefore, the acceleration calculations in (4) and (5) are given for an inertial coordinate system that coincides with the x and y directions at the moment. The side-slip angle, β , of the vehicle motion is defined as

$$\beta = \arctan \left(\frac{V_x}{V_y} \right), \quad (6)$$

where V_x and V_y are the velocity components of the vehicle measured in the $[x, y, z]$ coordinate system. Furthermore, the derivative of the yaw rate, \dot{r} , can be calculated as

$$\begin{aligned} \dot{r} &= \frac{1}{I_z} \left(\frac{w}{2} (F_{xf\bar{r}} + F_{xr\bar{r}} - F_{xfl} - F_{xrl}) \right. \\ &\quad \left. + (F_{yfl} + F_{yf\bar{r}})a - (F_{yrl} + F_{yr\bar{r}})b \right), \end{aligned} \quad (7)$$

where I_z is the moment inertia about the z axis, w is the width of the wheelbase, and a , b are the distances between the center of gravity and front and rear wheels, respectively (see Fig. 2a).

Wheel assembly, including the tire, is responsible for creating the traction forces for vehicle acceleration or deceleration. As the wheel spins with the torque input, the rotation starts, and the resulting slip between tire and road causes the traction force. Wheel dynamics are typically represented with the rotation of the tire about its lateral axis (traction) and the vertical axis (steering). For this work, it is assumed that the driver steering input is realized without any transient dynamics. The rotational dynamics equation about the lateral axis, for each wheel, can be obtained as

$$I_w \dot{\omega}_{ij} = T_{ij} - T_{bij} - T_{rij} - F_{xij} R_w, \quad (8)$$

where, ω_{ij} , T_{rij} , T_{ij} , and T_{bij} , are the angular velocity, rolling resistance, motor, and brake torques, respectively, that are applied on the wheel ij , $i \in \{f, r\}$, $j \in \{l, \bar{r}\}$. The rolling resistance, which originates from the deformable nature of the tire [33] is calculated as

$$T_{rij} = p_0 N_{ij} + p_1 N_{ij} \frac{V_x}{30} + p_2 N_{ij} \frac{V_x^4}{30^4}, \quad (9)$$

where, N_{ij} is the normal force acting on tire ij . The coefficients p_0 , p_1 and p_2 are usually obtained experimentally and typical values can be found in [34]. In order to calculate the longitudinal and lateral forces, f_{xij} and f_{yij} , respectively, on the tire, a friction model is required. In this work, Pacejka's Magic tire formula [35] is used. According to this formula, longitudinal traction force f_{xij} can be calculated as

$$f_{xij} = D_1 \sin[C_1 \arctan(B_1 \lambda_{ij} - E_1 (B_1 \lambda_{ij} - \arctan(B_1 \lambda_{ij})))], \quad (10)$$

where D_1 is the peak value, C_1 is the shape factor, B_1 is the stiffness factor and E_1 is the curvature factor. The longitudinal slip, λ_{ij} , in (10) is calculated separately for driving and braking conditions as

$$\begin{aligned} \text{For driving;} \quad \lambda_{ij}(V_x, w_{ij}) &= \frac{w_{ij} R_w - V_x}{w_{ij} R_w} \\ \text{For braking;} \quad \lambda_{ij}(V_x, w_{ij}) &= \frac{w_{ij} R_w - V_x}{V_x}, \end{aligned} \quad (11)$$

where V_x is the vehicle longitudinal velocity, w_{ij} is the rotational velocity on wheel ij , $i \in \{f, r\}$, $j \in \{l, \bar{r}\}$, and R_w is the radius of the wheel. The slip ratios, $\alpha_{ij}(V_x, V_y, r)$, for each tire, can be calculated using vehicle geometry as

$$\begin{aligned} \alpha_{fl}(V_x, V_y, r) &= \delta_{fl} - \arctan\left(\frac{V_y + r a \cos(\gamma_f)}{V_x - r a \sin(\gamma_f)}\right) \\ \alpha_{f\bar{r}}(V_x, V_y, r) &= \delta_{f\bar{r}} - \arctan\left(\frac{V_y + r a \cos(\gamma_f)}{V_x + r a \sin(\gamma_f)}\right) \\ \alpha_{rl}(V_x, V_y, r) &= \delta_{rl} - \arctan\left(\frac{V_y - r b \cos(\gamma_r)}{V_x - r b \sin(\gamma_r)}\right) \\ \alpha_{r\bar{r}}(V_x, V_y, r) &= \delta_{r\bar{r}} - \arctan\left(\frac{V_y - r b \cos(\gamma_r)}{V_x + r b \sin(\gamma_r)}\right). \end{aligned} \quad (12)$$

In (12), δ_{ij} is the steering angle on wheel ij , $i \in \{f, r\}$, $j \in \{l, \bar{r}\}$. The front and rear hub angles, γ_f and γ_r , are shown in Fig. 2. Finally, the lateral forces, f_{yij} , can be calculated by applying the Magic Formula given [35] as

$$f_{yij} = D_2 \sin[C_2 \arctan(B_2 \alpha_{ij} - E_2 (B_2 \alpha_{ij} - \arctan(B_2 \alpha_{ij})))]. \quad (13)$$

B. Vertical Dynamics

One of the main challenges of designing a comfortable car is finding suspension parameters that provide a balance between comfort and handling. A vertical model integrated with the handling model is needed to consider these two performance requirements simultaneously (see Fig. 2). The vertical dynamics model in this study is developed in two parts. First, equations of motion for sprung mass, which is the vehicle body supported by springs, are written. Then, unsprung

masses, which are the wheels that are excited from road disturbances, are modeled. It is assumed that the suspension system has a linear spring and a damper, while the tire is assumed to act as a linear spring [36].

Using the pitch, θ , and the roll, ϕ , angles the sprung mass elevation at each wheel location, z_{sij} , can be calculated as

$$z_{sfl} = z - a \sin(\theta) + 0.5w \sin(\phi), \quad (14)$$

$$z_{sf\bar{r}} = z - a \sin(\theta) - 0.5w \sin(\phi), \quad (15)$$

$$z_{srl} = z + b \sin(\theta) + 0.5w \sin(\phi), \quad (16)$$

$$z_{sf\bar{r}} = z + b \sin(\theta) - 0.5w \sin(\phi), \quad (17)$$

where z is the elevation of the center of mass (heave).

Using Fig. 2, the heave acceleration (\ddot{z}) can be calculated as

$$\begin{aligned} \ddot{z} &= \frac{1}{m} ((2k_{sf} + 2k_{sr})z - (2c_{sf} + 2c_{sr})\dot{z} \\ &\quad + (2ak_{sf} - 2bk_{sr}) \sin(\theta) + (2ac_{sf} - 2bc_{sr})\dot{\theta} \cos(\theta) \\ &\quad + k_{sf} z_{ufl} + c_{sf} \dot{z}_{ufl} + k_{sf} z_{uf\bar{r}} + c_{sf} \dot{z}_{uf\bar{r}} \\ &\quad + k_{sr} z_{url} + c_{sr} \dot{z}_{url} + k_{sr} z_{ur\bar{r}} + c_{sr} \dot{z}_{ur\bar{r}} \\ &\quad + f_{zf\bar{r}} + f_{zfl} + f_{zr\bar{r}} + f_{zfl}), \end{aligned} \quad (18)$$

where k_{sf} and c_{sf} are the front sprung mass spring and damping coefficients, k_{sr} and c_{sr} are the rear sprung mass spring and damping coefficients, respectively. z_{uij} is the unsprung mass displacement and f_{ij} is the active suspension forces at wheel ij , $i \in \{f, r\}$, $j \in \{l, \bar{r}\}$. Using Fig. 2b, the pitch acceleration $\ddot{\theta}$ can be calculated as

$$\begin{aligned} \ddot{\theta} &= \frac{1}{I_y} ((2ak_{sf} - 2bk_{sr})z + (2ac_{sf} - 2bc_{sr})\dot{z} \\ &\quad - (2a^2k_{sf} + 2b^2k_{sr}) \sin(\theta) - (2a^2c_{sf} + 2b^2c_{sr})\dot{\theta} \cos(\theta) \\ &\quad - ak_{sf} z_{ufl} - ac_{sf} \dot{z}_{ufl} - ak_{sf} z_{uf\bar{r}} - ac_{sf} \dot{z}_{uf\bar{r}} \\ &\quad + bk_{sr} z_{url} + bc_{sr} \dot{z}_{url} + bk_{sr} z_{ur\bar{r}} + bc_{sr} \dot{z}_{ur\bar{r}} \\ &\quad - ma_x h - af_{zfl} - af_{zf\bar{r}} + bf_{zrl} + bf_{zr\bar{r}}). \end{aligned} \quad (19)$$

Similarly, the roll acceleration $\ddot{\phi}$ can be calculated as

$$\begin{aligned} \ddot{\phi} &= \frac{1}{I_x} (-0.25w^2(2k_{sf} + 2k_{sr}) \sin(\phi) + 0.5wk_{sf} z_{ufl} \\ &\quad - 0.25w^2(2c_{sf} + 2c_{sr})\dot{\phi} \cos(\phi) + 0.5wc_{sf} \dot{z}_{ufl} \\ &\quad - 0.5wk_{sf} z_{uf\bar{r}} - 0.5wc_{sf} \dot{z}_{uf\bar{r}} + 0.5wk_{sr} z_{url} \\ &\quad + 0.5wc_{sr} \dot{z}_{url} - 0.5wk_{sr} z_{ur\bar{r}} - 0.5wc_{sr} \dot{z}_{ur\bar{r}} \\ &\quad - ma_y h + \frac{w}{2} f_{zfl} - \frac{w}{2} f_{zf\bar{r}} + \frac{w}{2} f_{zrl} - \frac{w}{2} f_{zr\bar{r}}). \end{aligned} \quad (20)$$

Elevation of each unsprung mass, z_{uij} , $i \in \{f, r\}$, $j \in \{l, \bar{r}\}$, can be calculated by using the forces acting on the wheels as

$$\begin{aligned} m_{uf} \ddot{z}_{ufl} &= k_{sf} z + c_{sf} \dot{z} - ak_{sf} \sin(\theta) - ac_{sf} \dot{\theta} \cos(\theta) \\ &\quad + 0.5wk_{sf} \sin(\phi) + 0.5wc_{sf} \dot{\phi} \cos(\phi) \\ &\quad - (k_{sf} + k_{uf}) z_{ufl} - c_{sf} \dot{z}_{ufl} \\ &\quad + k_{uf} z_{rfl} - f_{zfl}, \end{aligned} \quad (21)$$

$$\begin{aligned}
m_{uf}\ddot{z}_{ufr} &= k_{sf}z + c_{sf}\dot{z} - ak_{sf}\sin(\theta) - ac_{sf}\dot{\theta}\cos(\theta) \\
&\quad - 0.5wk_{sf}\sin(\phi) - 0.5wc_{sf}\dot{\phi}\cos(\phi) \\
&\quad - (k_{sf} + k_{uf})z_{ufl} - c_{sf}\dot{z}_{ufr} \\
&\quad + k_{uf}z_{rfr} - f_{zf\bar{r}},
\end{aligned} \tag{22}$$

$$\begin{aligned}
m_{ur}\ddot{z}_{url} &= k_{sr}z + c_{sr}\dot{z} + ak_{sr}\sin(\theta) + ac_{sr}\dot{\theta}\cos(\theta) \\
&\quad + 0.5wk_{sr}\sin(\phi) + 0.5wc_{sr}\dot{\phi}\cos(\phi) \\
&\quad - (k_{sr} + k_{ur})z_{url} - c_{sr}\dot{z}_{url} \\
&\quad + k_{ur}z_{rrl} - f_{zr\bar{l}},
\end{aligned} \tag{23}$$

and

$$\begin{aligned}
m_{ur}\ddot{z}_{urr} &= k_{sr}z + c_{sr}\dot{z} + ak_{sr}\sin(\theta) + ac_{sr}\dot{\theta}\cos(\theta) \\
&\quad - 0.5wk_{sr}\sin(\phi) - 0.5wc_{sr}\dot{\phi}\cos(\phi) \\
&\quad - (k_{sr} + k_{ur})z_{urr} - c_{sr}\dot{z}_{urr} \\
&\quad + k_{ur}z_{rrr} - f_{zr\bar{r}},
\end{aligned} \tag{24}$$

where, z_{rij} is the road disturbance at wheel ij , m_{uf} , m_{ur} , k_{uf} and k_{ur} are the sprung masses and the unsprung spring coefficients at the front and the rear tires, respectively. Finally, the normal forces at each tire can be calculated as

$$N_{ij} = k_{si}(z_{uij} - z_{rij}), \tag{25}$$

where N_{ij} is the normal force at tire ij .

Fig. 4 summarizes the interaction among many components of the resulting vehicle model developed in (1)-(25). The inputs of the model are the wheel torque, T_{ij} , the steering angle, δ_{ij} and the road excitation, z_{rij} , at each wheel, and the outputs are the all six translational and rotational motions of the vehicle as well as the rotation of the wheels and the deflections at the wheels and suspensions.

The proposed model presented in (1)-(25) is validated against the multi-body dynamics based commercial software [29] and found in good correlation for the driving conditions used in this work. Results for the validation studies can be found in [37].

III. CONTROL STRUCTURE

The overall closed-loop system, including the proposed control structure, is given in Fig. 5. In this structure, the driver provides the steering and the desired traction torque (based on the pedal position) inputs. These inputs are used by the controller to produce the virtual control input vector, containing the desired traction force, F_c , and the desired pitch, roll, and yaw moment corrections, namely M_x , M_y and M_z , respectively. Moreover, to ensure yaw stability, the desired lateral force correction, F_{yc} , is also calculated as another component of the virtual control input vector. The proposed control allocation algorithm determines the torque T_{ij} to be applied at each wheel, the rear-wheel steering angles δ_{rl} , $\delta_{r\bar{r}}$, the front-wheel steering angle corrections $\Delta\delta_{fl}$, $\Delta\delta_{f\bar{r}}$, and the active suspension forces f_{ij} , $i \in \{f, r\}$, $j \in \{l, \bar{r}\}$, based on the virtual control input vector.

A. Virtual Control Input Generation

In this section, calculation of the virtual control input vector elements, which are the desired traction force F_c , desired yaw, roll and pitch moment corrections M_z , M_x , M_y , and the required lateral force correction, F_{yc} , is described. The traction force command, F_c , is calculated using a Proportional Integral (PI) controller to ensure that the vehicle maintains the desired longitudinal acceleration:

$$\begin{aligned}
\tilde{F} &= F_{ref} - F \\
F_c &= K_{if} \int \tilde{F} dt + K_{pf} \tilde{F},
\end{aligned} \tag{26}$$

where F_{ref} is the traction force mapped from the pedal input of the driver, F is the vehicle traction force, and K_p and K_i are the PI controller gains.

To follow the steering input of the driver, first, a reference yaw rate, r_{ref} , is calculated using the methods proposed in [38] and [2]. Then, by defining the error, $\tilde{r} = r_{ref} - r$, between r_{ref} and the measured yaw rate, r , a moment, M_1 , is generated as

$$M_1 = K_{pmz}\tilde{r} + K_{imz} \int \tilde{r} dt, \tag{27}$$

where K_{pmz} and K_{imz} are the PI controller gains. Additionally, to ensure stability while following the yaw rate reference, side-slip angle β is fed to another PI controller to produce an additional moment, M_2 , as

$$M_2 = K_{ps}\beta + K_{is} \int \beta dt, \tag{28}$$

where, K_{ps} , K_{is} are the PI controller gains. Moments M_1 and M_2 are then summed to create the desired yaw moment correction M_z .

$$M_z = M_1 + M_2. \tag{29}$$

Lateral and longitudinal accelerations may cause the vehicle to roll and pitch. These motions are not desirable since they shift the center of gravity and may disturb the vehicle's stability. Therefore, to damp the roll and pitch motions, roll and pitch moment corrections, M_x and M_y , are calculated by using a PI controller as

$$\begin{aligned}
M_x &= -K_{pr}\phi - K_{dr}\dot{\phi} - K_{ir} \int \phi dt \\
M_y &= -K_{pp}\theta - K_{dp}\dot{\theta} - K_{ip} \int \theta dt,
\end{aligned} \tag{30}$$

where ϕ and θ are the roll and pitch angles of the vehicle and K_{pr} , K_{dr} , K_{ir} , K_{pp} , K_{dp} and K_{ip} are the PID controller gains.

The side-slip angle, β , should be kept small since a large value causes the vehicle to be unstable [25]. β can be controlled by applying a lateral force F_{yc} , which can be calculated as

$$F_{yc} = -K_{py}\beta - K_{iy} \int \beta, \tag{31}$$

where K_{py} and K_{iy} are the PI controller constants.

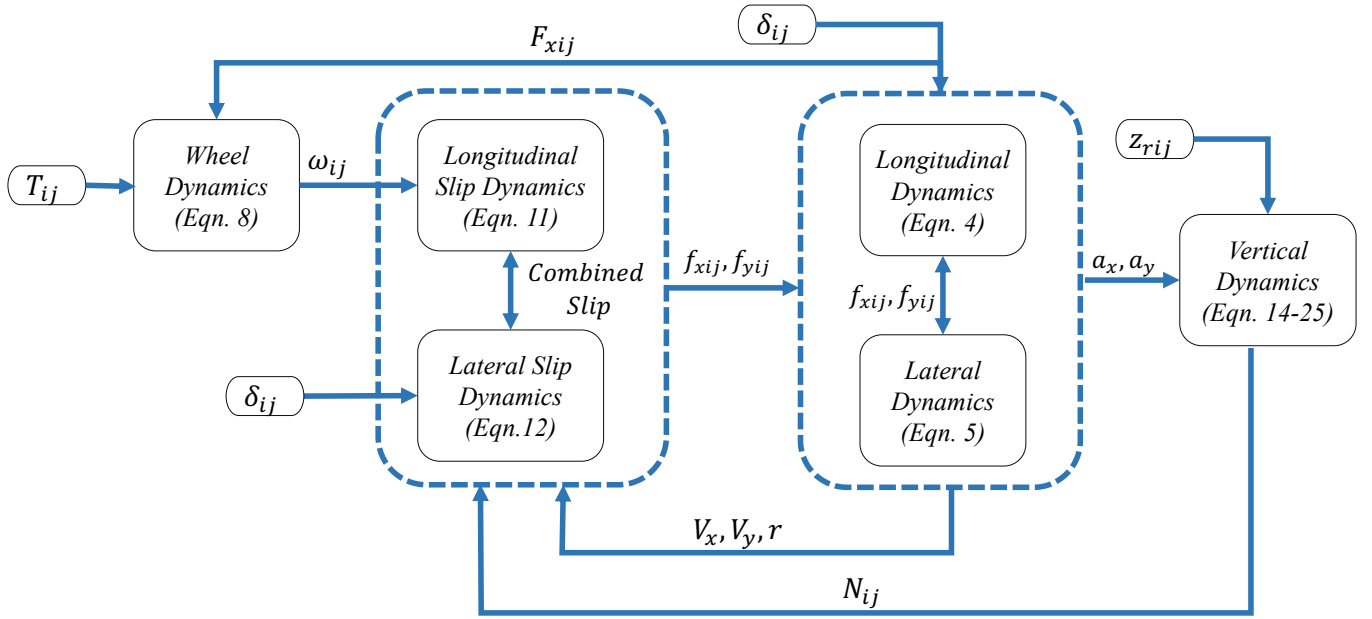


Fig. 4: Vehicle Model and Its Components

B. Vehicle Model for Control Allocation

In order to develop a control allocator, a control allocation oriented model is derived from the nonlinear vehicle dynamics model presented in Section II.

The vehicle outputs, which are used in the feedback loop (see Fig. 5), are the vehicle acceleration, a_x , the vehicle velocity, V , yaw rate, r , roll angle, ϕ , pitch angle, θ , and the wheel hub elevations, z_{uij} , $i \in \{f, r\}$, $j \in \{l, \bar{r}\}$. The states of the control-oriented model, which are the minimum number of variables the initial conditions of which are required to be known to predict the future behavior of the vehicle outputs, are then determined as

$$\mathbf{x}^T = [V_x \ V_y \ \dot{\psi} \ z \ \dot{z} \ \phi \ \dot{\phi} \ \theta \ \dot{\theta} \ z_{ufl} \ \dot{z}_{ufl} \ z_{uf\bar{r}} \ \dot{z}_{uf\bar{r}} \ z_{url} \ \dot{z}_{url} \ z_{ur\bar{r}} \ \dot{z}_{ur\bar{r}}]. \quad (32)$$

Using these states, non-linear dynamics of the vehicle given in (1)-(25) can be represented in the form,

$$\dot{\mathbf{x}} = f(\mathbf{x}, \mathbf{u}), \quad (33)$$

where the state vector, \mathbf{x} , is given in (32), and the actuator input vector, \mathbf{u} , is

$$\mathbf{u}^T = \begin{bmatrix} \delta_{fl} & \delta_{f\bar{r}} & \delta_{rl} & \delta_{r\bar{r}} & T_{fl} & T_{f\bar{r}} \\ T_{rl} & T_{r\bar{r}} & f_{zfl} & f_{zf\bar{r}} & f_{zrl} & f_{zr\bar{r}} \end{bmatrix}. \quad (34)$$

Assuming a constant cruising velocity V_0 , and small steering (δ_{ij}) and tire slip angles (α_{ij}), a linearized time-varying vehicle model can be obtained in the form

$$\dot{\mathbf{x}} = \mathbf{A}\mathbf{x} + \mathbf{B}_u(t)\mathbf{u} + \mathbf{D}, \quad (35)$$

where $\mathbf{A} \in R^{17 \times 17}$ is the state matrix, $\mathbf{B}_u(t) \in R^{17 \times 12}$

is the time varying input matrix and $\mathbf{D} \in R^{17}$ contains the disturbances. The contents of the matrices \mathbf{A} , $\mathbf{B}_u(t)$, and \mathbf{D} are available online ¹.

To treat the elements of \mathbf{u} given in (34) as pure force and moment generators, and hence make the representation suitable for control allocation, rows of the input matrix B_u that corresponds to the variations in heave, z , and unsprung mass, z_{uij} , elevations are taken to be zero. This assumption ignores the effects of active suspension forces on the vehicle body and unsprung mass accelerations. This is a common practice for control allocation implementations, the examples of which can be seen at [9], [39], [40]. It is noted that the linear time-varying dynamics (35) is used only for control allocation development purposes. For the controller validation tests, the full nonlinear model developed in Section II is employed.

C. Control Allocation

The exploited control allocation method is based on [30], and the block diagram for this algorithm, modified for the specific application considered in this paper, is given in Fig. 6. For the vehicle control application studied in this paper, the algorithm is re-worked such that it can handle the time-varying input matrix $B_u(t)$ introduced in (35).

Rewriting \mathbf{u} as a summation of the driver input, $\Delta\mathbf{u}$, and the control allocation input, \mathbf{u}_{ca} , (i.e. $\mathbf{u} \equiv \mathbf{u}_{ca} + \Delta\mathbf{u}$), (35) can be rewritten as

$$\dot{\mathbf{x}} = \mathbf{A}\mathbf{x} + \mathbf{B}_u(t)\mathbf{u}_{ca} + \mathbf{B}_u(t)\Delta\mathbf{u} + \mathbf{D}, \quad (36)$$

¹https://github.com/otemiz/Adaptive_control_allocation

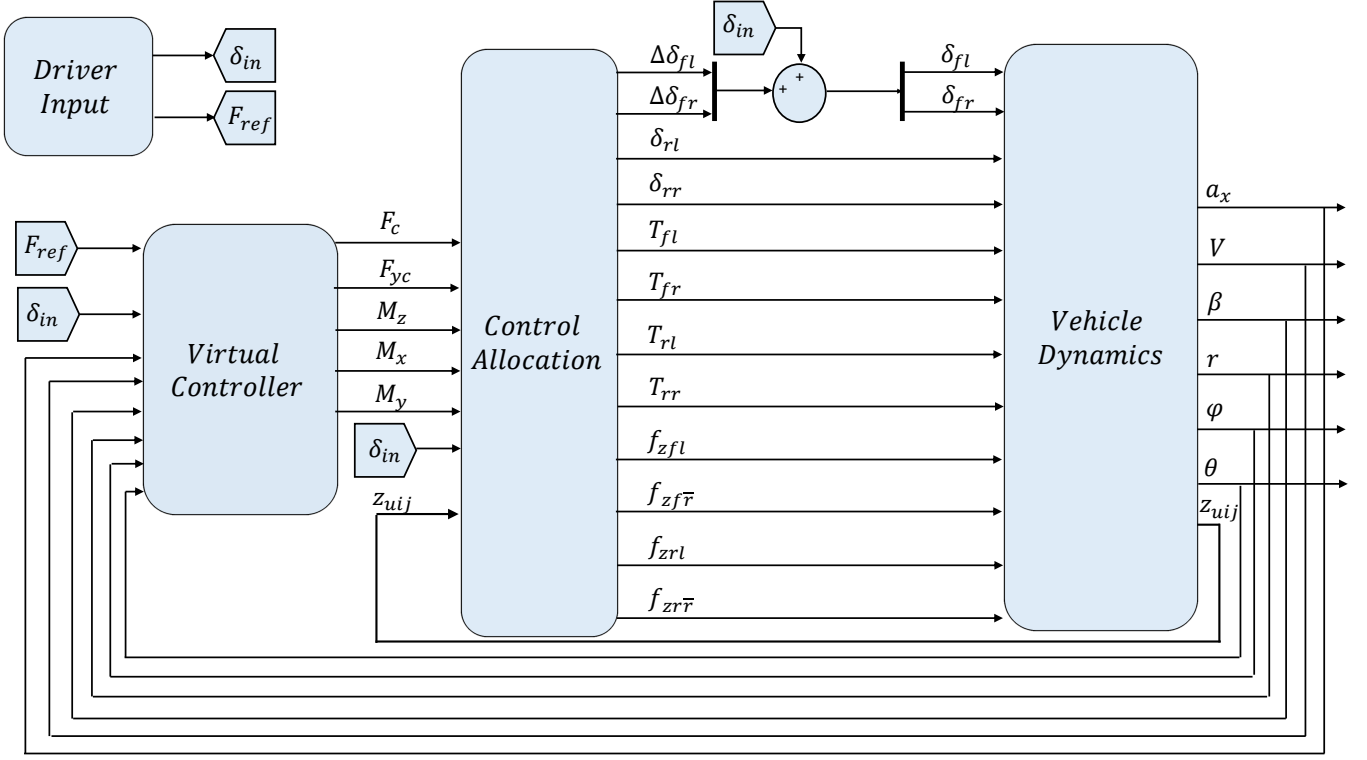


Fig. 5: Overall Closed Loop System

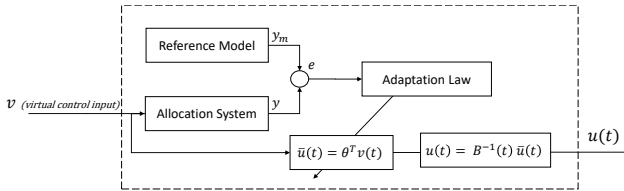


Fig. 6: Control Allocation Structure

(39) can be rewritten as

$$\dot{\mathbf{x}} = \mathbf{A}\mathbf{x} + \mathbf{B}_v[\mathbf{B}_y(t)\mathbf{u}_{ca} + \bar{\mathbf{d}}]. \quad (41)$$

The time-varying matrix $\mathbf{B}_y(t)$ can be written as a multiplication of a constant matrix, \mathbf{B}_1 , and a time-varying invertible matrix $\mathbf{B}_n(t)$, as $\mathbf{B}_y(t) = \mathbf{B}_1\mathbf{B}_n(t)$, where the contents of the matrices, $\mathbf{B}_1 \in R^{5 \times 12}$ and $\mathbf{B}_n(t) \in R^{12 \times 12}$ are given in Appendix A. Then, this multiplication can be substituted into (41) to obtain

$$\dot{\mathbf{x}} = \mathbf{A}\mathbf{x} + \mathbf{B}_v[\mathbf{B}_1\mathbf{B}_n(t)\mathbf{u}_{ca} + \bar{\mathbf{d}}]. \quad (42)$$

Defining $\bar{\mathbf{u}} \equiv \mathbf{B}_n(t)\mathbf{u}_{ca}$, and introducing a diagonal unknown matrix $\Lambda \in R^{12 \times 12}$ with positive entries, the state equation given in (42) can be rewritten as

$$\dot{\mathbf{x}} = \mathbf{A}\mathbf{x} + \mathbf{B}_v(\mathbf{B}_1\Lambda\bar{\mathbf{u}} + \bar{\mathbf{d}}) \quad (43)$$

$$= \mathbf{A}\mathbf{x} + \mathbf{B}_v\mathbf{v}, \quad (44)$$

where $\mathbf{v} \in R^5$ is the virtual control input consisting of the desired forces and moments derived in Section III-A. It is noted that faults and uncertainties in actuator effectiveness can be represented with the help of Λ . The objective of the control allocation is to determine the vector \mathbf{u} to achieve

$$\mathbf{B}_1\Lambda\bar{\mathbf{u}} + \bar{\mathbf{d}} = \mathbf{v}, \quad (45)$$

where $\mathbf{B}_1\Lambda\bar{\mathbf{u}} + \bar{\mathbf{d}}$ represents the net forces moments acting on the vehicle, which can be measured using an inertial measurement unit.

In order to build the mechanism for control allocation, we

where

$$\Delta\mathbf{u}^T = \begin{bmatrix} \delta_{in} & \delta_{in} & 0 & 0 & 0 & 0 \\ 0 & 0 & 0 & 0 & 0 & 0 \end{bmatrix}, \quad (37)$$

$$\mathbf{u}_{ca}^T = \begin{bmatrix} \Delta\delta_{fl} & \Delta\delta_{fr} & \delta_{rl} & \delta_{rr} & T_{fl} & T_{fr} \\ T_{rl} & T_{rr} & f_{zfl} & f_{zfr} & f_{zrl} & f_{zrr} \end{bmatrix}.$$

In accordance with this decomposition, $\mathbf{B}_u(t)$ can be split into matrices $\mathbf{B}_v \in R^{17 \times 5}$ and $\mathbf{B}_y(t) \in R^{5 \times 12}$, as $\mathbf{B}_u(t) = \mathbf{B}_v\mathbf{B}_y(t)$. Matrices \mathbf{B}_v and $\mathbf{B}_y(t)$ are given in Appendix A. Using this decomposition, (36) can be rewritten as

$$\dot{\mathbf{x}} = \mathbf{A}\mathbf{x} + \mathbf{B}_v\mathbf{B}_y(t)(\mathbf{u}_{ca} + \Delta\mathbf{u}) + \mathbf{D}. \quad (38)$$

Writing \mathbf{D} as $\mathbf{D} = \mathbf{B}_v\mathbf{d}$, where the entries of the vector \mathbf{d} is given in the Appendix A, expression in (38) can be rewritten as

$$\dot{\mathbf{x}} = \mathbf{A}\mathbf{x} + \mathbf{B}_v[\mathbf{B}_y(t)(\mathbf{u}_{ca} + \Delta\mathbf{u}) + \mathbf{d}] \quad (39)$$

$$= \mathbf{A}\mathbf{x} + \mathbf{B}_v[\mathbf{B}_y(t)\mathbf{u}_{ca} + \mathbf{B}_y(t)\Delta\mathbf{u} + \mathbf{d}].$$

Defining

$$\bar{\mathbf{d}} \equiv \mathbf{B}_y(t)\Delta\mathbf{u} + \mathbf{d}, \quad (40)$$

consider a dynamic system

$$\dot{\xi} = \mathbf{A}_m \xi + \mathbf{B}_1 \Lambda \bar{\mathbf{u}} + \bar{\mathbf{d}} - \mathbf{v}, \quad (46)$$

where $\mathbf{A}_m \in R^{5 \times 5}$ is stable. A reference model can also be defined as

$$\dot{\xi}_m = \mathbf{A}_m \xi_m. \quad (47)$$

$\bar{\mathbf{u}}$ can be created as $\bar{\mathbf{u}} = \boldsymbol{\theta}^T \mathbf{v}$, where $\boldsymbol{\theta} \in R^{12 \times 5}$ is a parameter matrix to be determined, and (46) can be rewritten as

$$\dot{\xi} = \mathbf{A}_m \xi + (\mathbf{B}_1 \Lambda \boldsymbol{\theta}^T - \mathbf{I}) \mathbf{v} + \bar{\mathbf{d}}. \quad (48)$$

Assuming an ideal parameter vector $\boldsymbol{\theta}^*$ that satisfies $\mathbf{B}_1 \Lambda \boldsymbol{\theta}^{*T} = \mathbf{I}$ and defining $\tilde{\boldsymbol{\theta}}^T \equiv \boldsymbol{\theta}^T - \boldsymbol{\theta}^{*T}$, where $\tilde{\boldsymbol{\theta}}$ is the deviation of the parameter vector $\boldsymbol{\theta}$ from its ideal value $\boldsymbol{\theta}^*$, (48) can be rewritten as

$$\dot{\xi} = \mathbf{A}_m \xi + \mathbf{B}_1 \Lambda \tilde{\boldsymbol{\theta}}^T \mathbf{v} + \bar{\mathbf{d}}. \quad (49)$$

Defining an error as $\mathbf{e} = \xi - \xi_m$ and subtracting (47) from (49), it is obtained that

$$\dot{\mathbf{e}} = \mathbf{A}_m \mathbf{e} + \mathbf{B}_1 \Lambda \tilde{\boldsymbol{\theta}}^T \mathbf{v} + \bar{\mathbf{d}}. \quad (50)$$

Theorem 1: If the parameter matrix $\boldsymbol{\theta}$ is updated with the adjustment law as,

$$\dot{\boldsymbol{\theta}} = \Gamma \text{Proj}(\boldsymbol{\theta}, -\mathbf{v} \mathbf{e}^T \mathbf{P} \mathbf{B}_1), \quad (51)$$

where $\Gamma = \mathbf{\Gamma}^T = \gamma \mathbf{I}_r \in R^{5 \times 5} > 0$, γ is a positive scalar, \mathbf{I}_r is an identity matrix, Proj refers to the projection operator [41], and \mathbf{P} is the positive definite symmetric solution of the Lyapunov equation $\mathbf{A}_m^T \mathbf{P} + \mathbf{P} \mathbf{A}_m = -\mathbf{Q}$, where \mathbf{Q} is a positive definite symmetric matrix, all the signals in the proposed control allocation structure given in (46)-(50) and (45) is achieved.

Proof: See [30], [31] and [32]

Theorem 2: The closed loop system, consisting of the plant (44), and the control input, \mathbf{v} , whose elements are given in (26) - (31), is stable.

Proof: See Appendix B.

IV. SIMULATIONS

In order to validate the proposed control framework, a Matlab/Simulink model of the overall closed-loop system is constructed. Different failure scenarios are simulated, and the results are compared with a baseline controller.

A. Baseline Controller

The baseline controller has three separate subsystems consisting of rear-wheel steering control, traction force control, and active suspension control.

1) *Rear Wheel Steering Control:* In the baseline controller, the rear wheel's angle of rotation is determined to be proportional to the front wheels' rotation angle. This proportion is determined based on the studies presented in [2], [42], where the amount of the gain, K_s , between the front and rear-wheel steering is tuned to improve stability and performance: At low speeds, K_s is negative to increase maneuverability. At high

speeds, however, the gain is positive, which increases stability. Specifically, K_s is determined as

$$K_s = \frac{\delta_r}{\delta_f} = \frac{mV_x^2 a - bLC_\alpha N_r}{mV_x^2 b + aLC_\alpha N_f} \cdot \frac{C_\alpha N_f}{C_\alpha N_r}, \quad (52)$$

where L is the length of the wheelbase, m is the vehicle mass, V_x is the longitudinal velocity, C_α is the lateral friction coefficient, N_f , N_r are normal forces at the front and rear tires, respectively and δ_f and δ_r are rear and front steering angles.

2) *Traction Control:* The total traction force, F_c , is generated using a PI controller similar to the one used in the proposed virtual control input given in (26). Then, this total traction force is distributed among the wheels proportional to the normal forces at the tires. The resulting control law can be written as

$$T_{ij} = \frac{F_c mg}{4N_{ij}}, \quad (53)$$

where mg is the weight of the vehicle, and T_{ij} and N_{ij} are the torque and the normal force at wheel ij , $i \in \{f, r\}$, $j \in \{l, \bar{r}\}$.

3) *Active Suspension Control:* For active suspension control, a similar approach given in [43] is used. Active suspension forces are determined by two PI controllers to stabilize the roll and pitch motions. PI controllers use the deviations of the roll, θ , and pitch, ϕ , angles to determine the required active suspension forces for stabilization. These forces are then distributed to the individual wheels, according to their moment creation effects provided in (19) and (20), as

$$f_{pitch} = -K_{pp}\theta - K_{ip} \int \theta dt \quad (54)$$

$$f_{roll} = -K_{pr}\phi - K_{ir} \int \phi dt$$

$$\begin{aligned} f_{zfl} &= -f_{pitch} + f_{roll} \\ f_{zfr} &= -f_{pitch} - f_{roll} \\ f_{zrl} &= f_{pitch} + f_{roll} \\ f_{zrr} &= f_{pitch} - f_{roll}, \end{aligned} \quad (55)$$

where f_{zij} , $i \in \{f, r\}$, $j \in \{l, \bar{r}\}$ is the active suspension force at wheel ij .

B. Low-Speed Performance

Initially, the proposed control framework is compared to the baseline controller for the case of no failure and when the initial velocity of the vehicle is set as $V_x = 13$ m/s. The scenario consists of an object avoidance maneuver followed by an emergency braking. The simulation results are given in Fig. 7, where the bottom sub-figure shows the trajectories of the vehicles with the baseline (w/o) and the proposed controllers (w/). In the sub-figure, the obstacle is represented by a pink dash-dotted line at $x = 100$ m. In this scenario, the steering maneuver starts at $t = 3$ s and ends at $t = 6$ s. Later, at $t = 6.5$ s driver brakes for 1 s and then driver gives no throttle or brake input. Fig. 7 also shows the allocated signals, which are steering angle corrections, $\Delta\delta_{ij}$, wheel torques T_{ij} , active suspension forces, f_{zij} , $i \in \{f, r\}$, $j \in \{l, \bar{r}\}$, and vehicle states $\mathbf{x} = [\beta \ V_x \ \psi \ \phi \ \theta]$. As seen from the figure, the

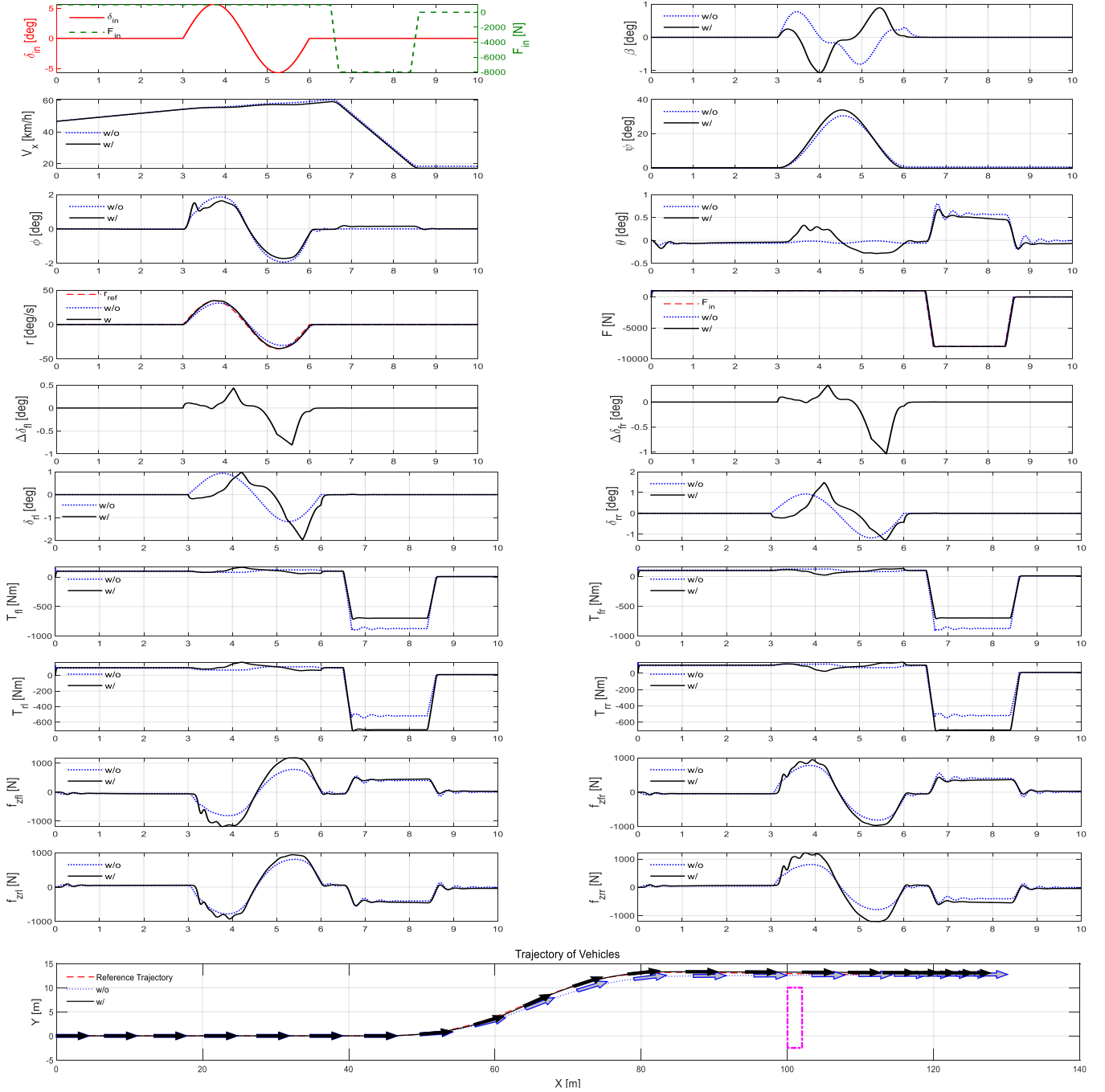


Fig. 7: Object Avoidance Maneuver in Low Velocity Scenario. "w/" and "w/o" refer to the cases with and without the proposed control framework, respectively.

proposed system performs similarly to the baseline system under low speed and no-fault conditions.

C. High-Speed Performance

In this scenario, the proposed controller is compared to the baseline system when the initial velocity, V_x , is 20 m/s. The same steering and acceleration/brake inputs are applied as the previous case, and there are no failures in the system. The simulation results are given in Fig. 8. When side-slip, β , values of the two vehicles are compared, it is seen that

the baseline vehicle has much less side-slip. This is due to the nature of the rear steering gain K_s , which is designed to maintain yaw stability. However, this reduces yaw rotation and prevents the vehicle from escaping the obstacle. On the other hand, the proposed control framework provides a better yaw rate reference following while also keeping the vehicle stable.

D. Performance in Varying Road Conditions

In this simulation, the road friction coefficient C_α for the right tires is reduced to 60% of its original value to simulate

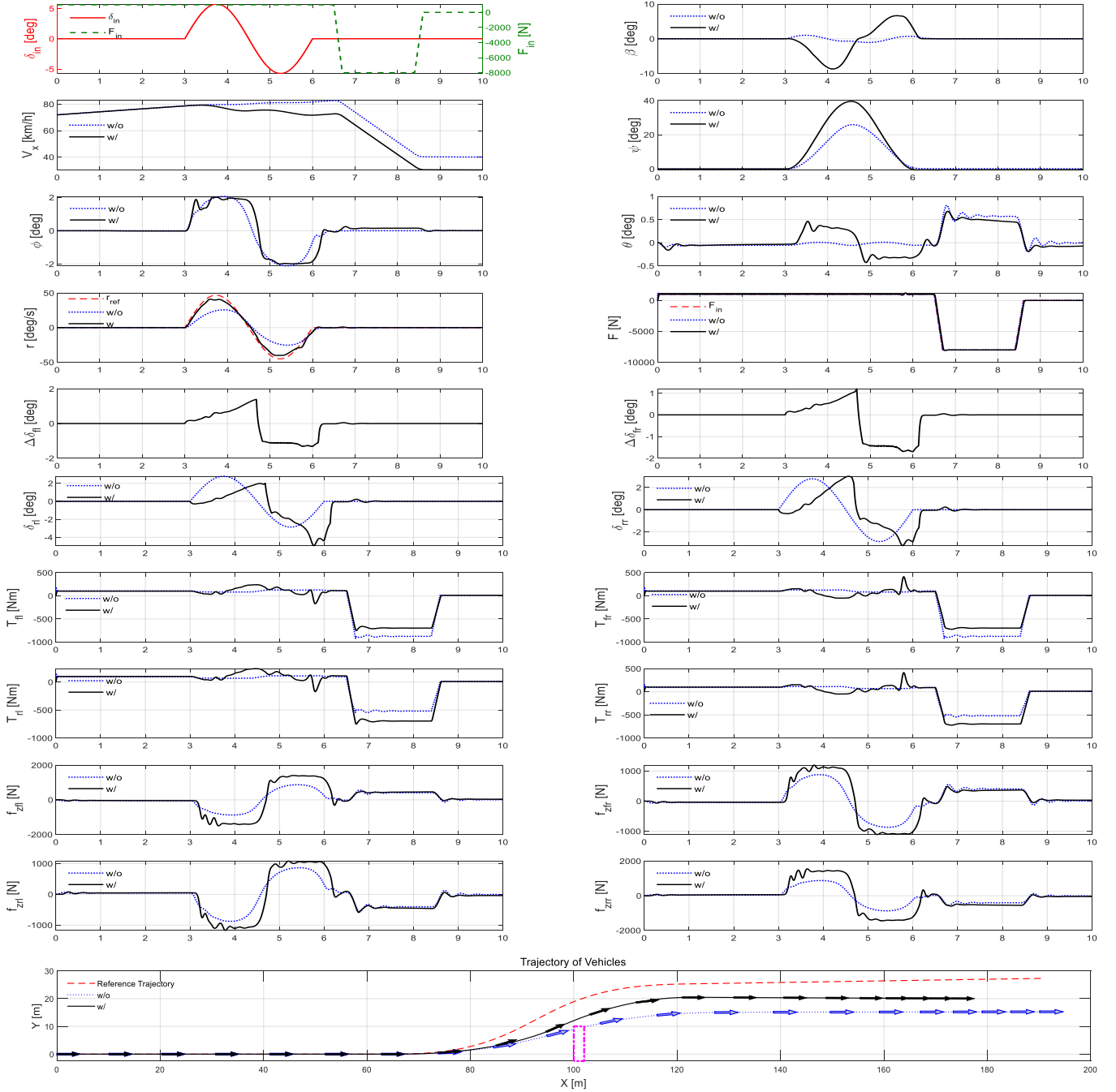


Fig. 8: Object Avoidance Maneuver in High-Velocity Scenario. "w/" and "w/o" refer to the cases with and without the proposed control framework, respectively.

slippery road conditions, starting at $t = 4$ s. The vehicle is commanded to perform the same object avoidance maneuver with an initial velocity of 20 m/s. The results in Fig. 9 show that the baseline vehicle has difficulty following the commands while the proposed controller performs as designed. In order to compensate for varying road conditions, the proposed system shifts torque distribution toward the right wheels. Moreover, trajectories, side slip angles, and velocities show that the vehicle equipped with the proposed controller remains stable, while the baseline system over-steers at the first steering input

and spins out of control.

E. Actuator Failure with Varying Road Conditions

In order to test the performance of the proposed controller in challenging situations, an "effectiveness loss at the wheel" scenario is created. In this scenario, the rear right tire traction force and steering angle are reduced to 10% of their original values, at $t = 1$ s. Additionally, at $t = 4$ s, the lateral friction coefficient is reduced by 10%. In the scenario, the initial velocity is also set to 20 m/s. The results of the simulation are

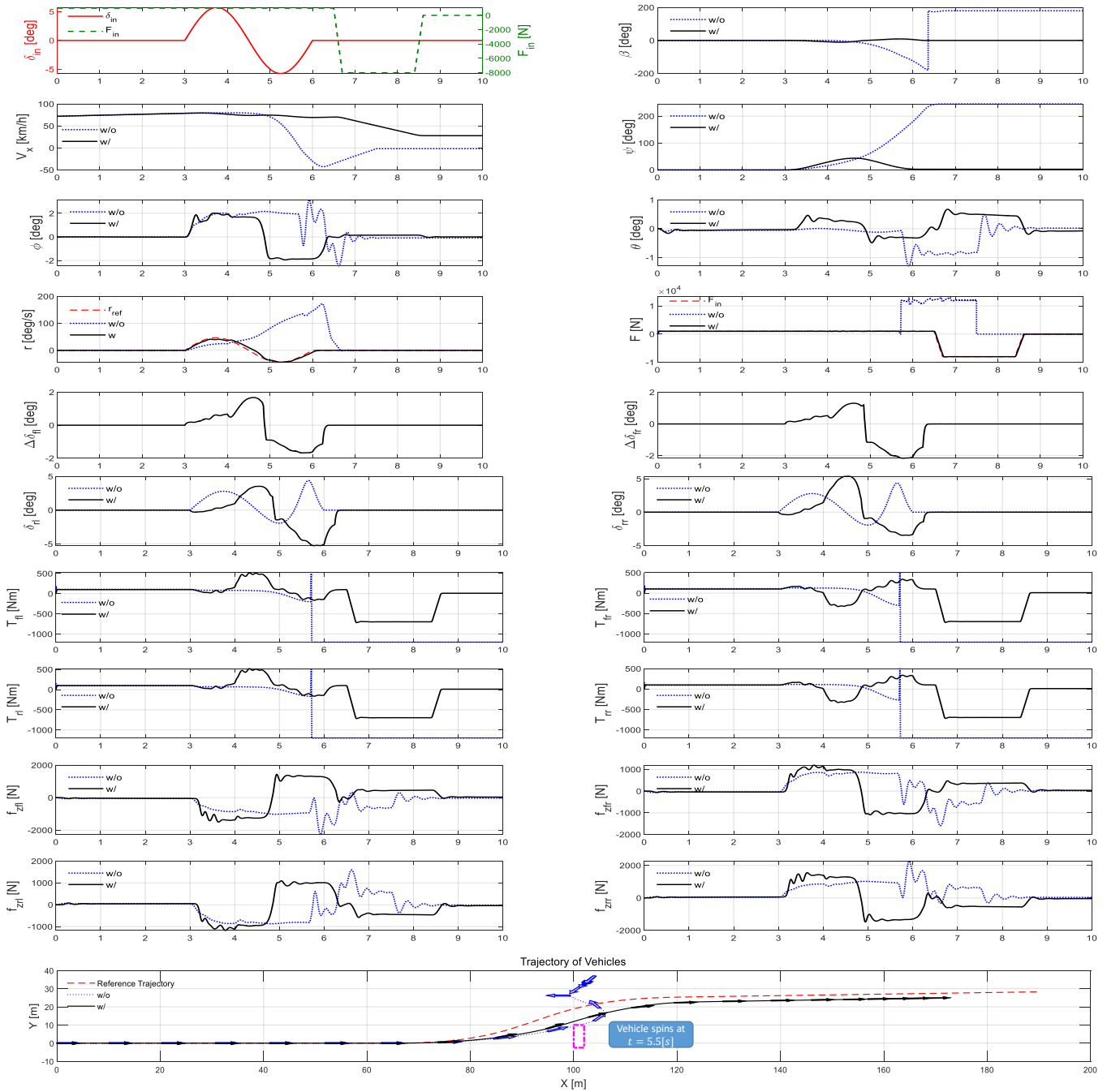


Fig. 9: Object Avoidance Maneuver with Varying Road Conditions. "w/" and "w/o" refer to the cases with and without the proposed control framework, respectively.

given in Fig. 10. The proposed controller modifies the steering angles to compensate for the undesired moments created by actuator effectiveness losses, which ensures a stable turn around the obstacle and a proper following of the reference trajectory. On the other hand, the baseline system cannot make a stable turn and spins. (It is observed that even for a lower initial velocity of 15 m/s, the baseline system loses stability.)

F. Integrated vs Independent Active Suspension

To demonstrate the advantages of an integrated active suspension system, the suspension control in the proposed control framework is replaced with that of the baseline controller, and the resulting structure is compared with the original integrated framework. The outcomes are presented in Fig. 11. In order to level the comparison, controller parameters are adjusted such that when there is no fault, the system performances are similar. In this scenario, the initial velocity is set to 20 m/s, and the effectiveness of the suspension actuators at the rear

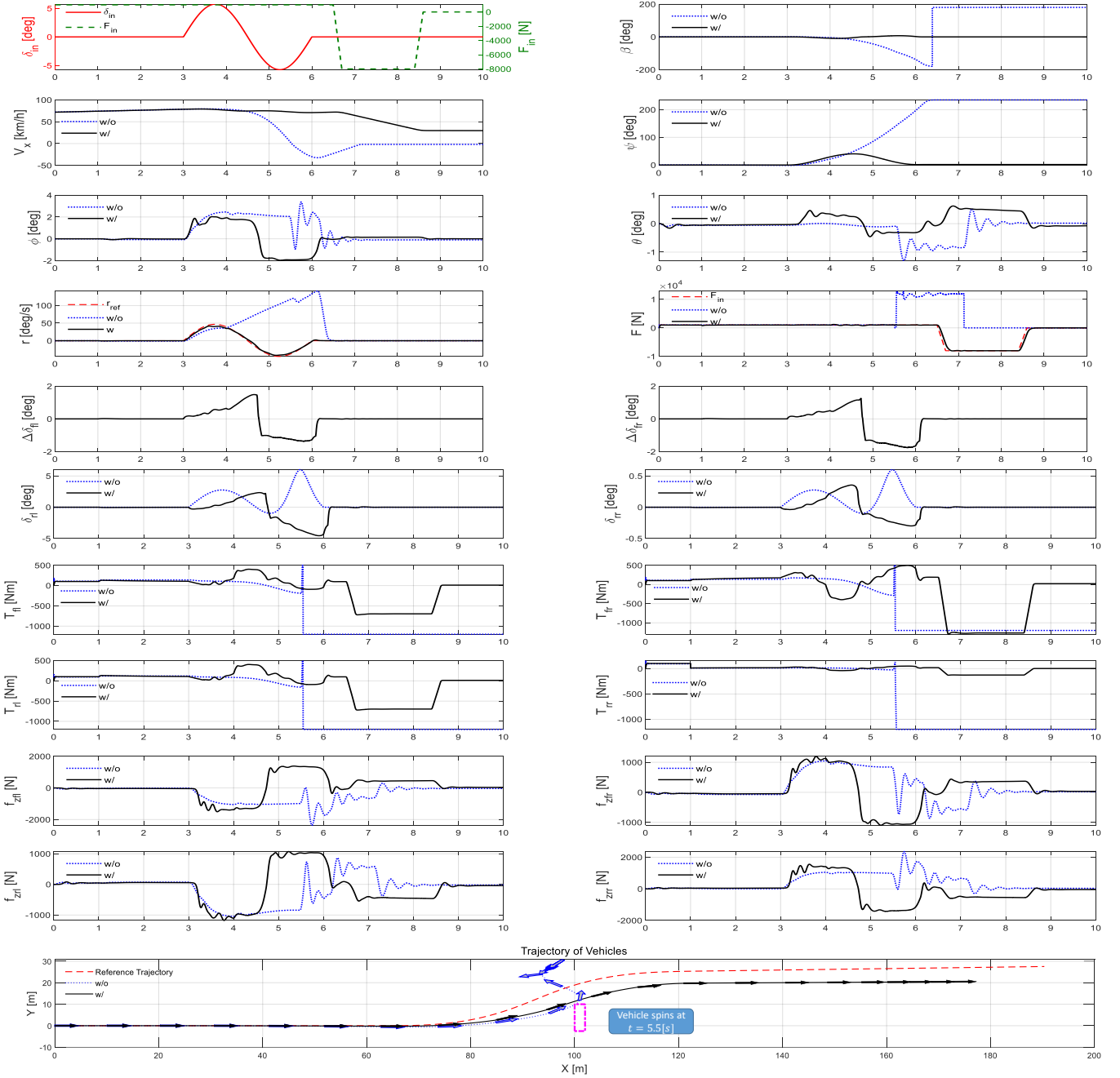


Fig. 10: Object Avoidance Maneuver with Actuator Failure and Varying Road Conditions. "w/" and "w/o" refer to the cases with and without the proposed control framework, respectively.

right wheel is reduced to 10% of its original value when $t = 1$ s. The proposed control framework increases the suspension force in the front left wheel f_{zl} , to compensate for the failure. As a result, despite the initial adaptation phase, the proposed scheme keeps the roll and pitch angles approximately 35% lower, compared to the case where the baseline controller is used for suspension control. It is noted that smaller roll and pitch angles result in a reduced shift in the center of gravity and a more stable and comfortable ride is achieved [2].

V. CONCLUSIONS

In this paper, a novel control framework is introduced as an integrated vehicle controller that can handle the uncertainties and non-linearities of the lateral and vertical dynamics of the vehicle motion. The framework is designed based on and validated by a 14 degrees of freedom model that incorporates steering, suspension, and forward motion dynamics. The controller employs steering, traction, and suspension forces to follow desired yaw and force references while keeping the vehicle stable under unfavorable driving conditions. Simulation results show that the presented framework provides a

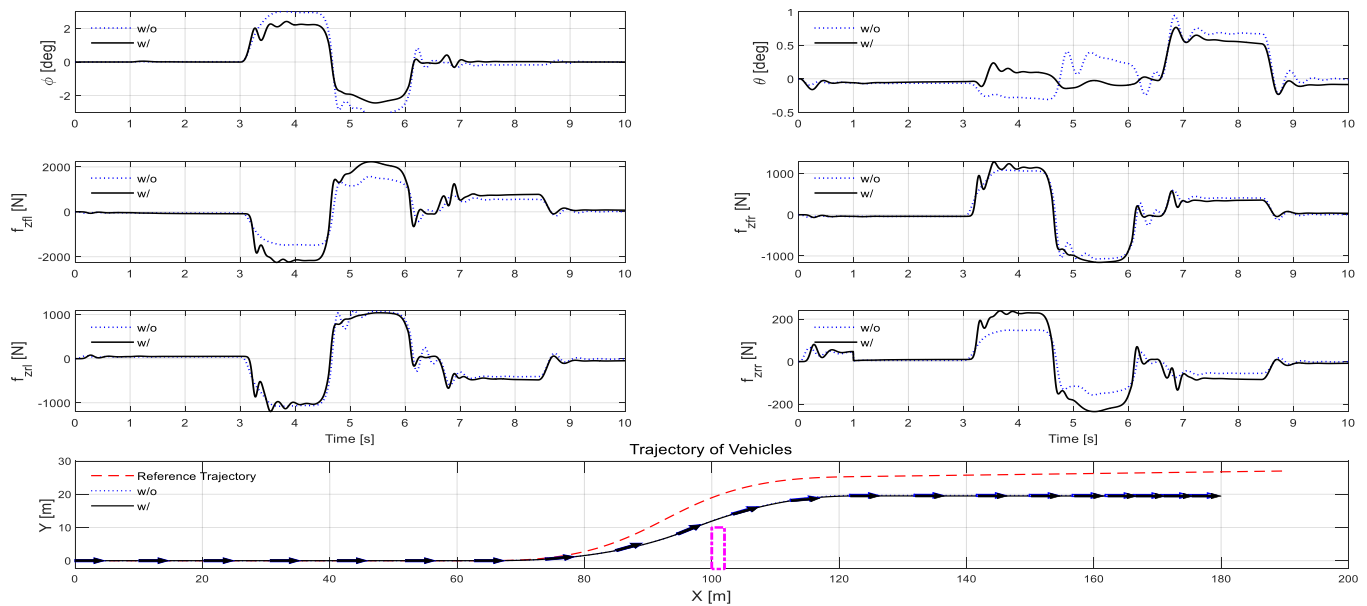


Fig. 11: Comparison of Active Suspensions in Case of Failure. "w/" and "w/o" refer to the cases with and without the proposed control framework, respectively.

comparable performance with the baseline system in a low-velocity and no-failure scenario. However, when the velocity is higher, the baseline system cannot perform as well as the proposed control framework. Moreover, when a fault or a road uncertainty is introduced, the proposed system can tolerate these non-ideal situations (up to 30% higher longitudinal maneuver velocity), whereas the baseline controller oversteers and makes the vehicle spin. Finally, our work shows that an integrated active suspension is better at overcoming a difficult maneuver with a better ride performance (approximately 35% lower roll and pitch angles during same steering conditions) compared to an independent suspension control.

REFERENCES

- [1] M. Cakmakci and A. G. Ulsoy, "Swappable Distributed MIMO Controller for a VCT Engine," *IEEE Transactions on Control Systems Technology*, vol. 19, no. 5, pp. 1168–1177, sep 2011.
- [2] A. G. Ulsoy, H. Peng, and M. Çakmakci, *Automotive Control Systems*. Cambridge University Press, 2012.
- [3] H. I. Dokuyucu and M. Cakmakci, "Concurrent Design of Energy Management and Vehicle Traction Supervisory Control Algorithms for Parallel Hybrid Electric Vehicles," *IEEE Transactions on Vehicular Technology*, vol. 65, no. 2, pp. 555–565, feb 2016.
- [4] M. Ataei, A. Khajepour, and S. Jeon, "A Novel Reconfigurable Integrated Vehicle Stability Control with Omni Actuation Systems," *IEEE Transactions on Vehicular Technology*, vol. 67, no. 4, pp. 2945–2957, 2018.
- [5] M. Mirzaei and H. Mirzaeinejad, "Fuzzy Scheduled Optimal Control of Integrated Vehicle Braking and Steering Systems," *IEEE/ASME Transactions on Mechatronics*, vol. 22, no. 5, pp. 2369–2379, 2017.
- [6] S. Fergani, O. Sename, and L. Dugard, "An LPV/H integrated Vehicle Dynamic Controller," *IEEE Transactions on Vehicular Technology*, vol. 65, no. c, pp. 1–1, 2015.
- [7] J. Ni, J. Hu, and C. Xiang, "Envelope Control for Four-Wheel Independently Actuated Autonomous Ground Vehicle Through AFS/DYC Integrated Control," *IEEE Transactions on Vehicular Technology*, vol. 66, no. 11, pp. 9712–9726, 2017.
- [8] T. A. Johansen and T. I. Fossen, "Control allocation - A survey," *Automatica*, vol. 49, no. 5, pp. 1087–1103, 2013.
- [9] O. Härkegård, "Backstepping and control allocation with applications to flight control," Ph.D. dissertation, Linköping University Linköping University, Department of Electrical Engineering, The Institute of Technology, 2003.
- [10] D. M. Acosta, Y. Yildiz, R. W. Craun, S. D. Beard, M. W. Leonard, G. H. Hardy, and M. Weinstein, "Piloted evaluation of a control allocation technique to recover from pilot-induced oscillations," *Journal of Aircraft*, vol. 52, no. 1, pp. 130–140, 2015.
- [11] Y. Yildiz and I. Kolmanovsky, "Stability properties and cross-coupling performance of the control allocation scheme capio," *Journal of Guidance, Control, and Dynamics*, vol. 34, no. 4, pp. 1190–1196, 2011.
- [12] E. Ono, Y. Hattori, Y. Muragishi, and K. Koibuchi, "Vehicle dynamics integrated control for four-wheel-distributed steering and four-wheel-distributed traction/braking systems," *Vehicle System Dynamics*, vol. 44, no. 2, pp. 139–151, 2006.
- [13] A. Tavasoli, M. Naraghi, and H. Shakeri, "Optimized coordination of brakes and active steering for a 4WS passenger car," *ISA Transactions*, vol. 51, no. 5, pp. 573–583, sep 2012.
- [14] R. Wang, H. Zhang, and J. Wang, "Linear parameter-varying controller design for four-wheel independently actuated electric ground vehicles with active steering systems," *IEEE Transactions on Control Systems Technology*, vol. 22, no. 4, pp. 1281–1296, 2014.
- [15] G. Yin, N. Chen, and P. Li, "Improving handling stability performance of four-wheel steering vehicle via μ -synthesis robust control," *IEEE Transactions on Vehicular Technology*, vol. 56, no. 5 I, pp. 2432–2439, 2007.
- [16] H. E. B. Russell and J. C. Gerdes, "Design of Variable Vehicle Handling Characteristics Using Four-Wheel Steer-by-Wire," *IEEE Transactions on Control Systems Technology*, vol. 24, no. 5, pp. 1529–1540, sep 2016.
- [17] M. W. Oppenheimer, D. B. Doman, and M. A. Bolender, "Control allocation for over-actuated systems," in *2006 14th Mediterranean Conference on Control and Automation*, June 2006, pp. 1–6.
- [18] Y. Yildiz and I. V. Kolmanovsky, "A control allocation technique to recover from pilot-induced oscillations (capio) due to actuator rate limiting," *Proceedings of the 2010 American Control Conference*, pp. 516–523, 2010.
- [19] Y. Yildiz, I. V. Kolmanovsky, and D. Acosta, "A control allocation system for automatic detection and compensation of phase shift due to actuator rate limiting," in *Proceedings of the 2011 American Control Conference*, 2011, pp. 444–449.
- [20] A. Wong, D. Kasinathan, A. Khajepour, S.-K. Chen, and B. Litkouhi, "Integrated torque vectoring and power management framework for electric vehicles," *Control Engineering Practice*, vol. 48, pp. 22 – 36, 2016.
- [21] J. Wang and R. G. Longoria, "Coordinated and reconfigurable vehicle

dynamics control,” *IEEE Transactions on Control Systems Technology*, vol. 17, no. 3, pp. 723–732, May 2009.

- [22] Y. Wang, G. Liu, D. Zhang, H. Zhou, H. Ye, and X. Chen, “Combined Fault-Tolerant Control with Optimal Control Allocation for Four-Wheel Independently Driven Electric Vehicles,” in *2016 IEEE Vehicle Power and Propulsion Conference (VPPC)*. IEEE, oct 2016, pp. 1–5.
- [23] Z. Shuai, H. Zhang, J. Wang, J. Li, and M. Ouyang, “Lateral motion control for four-wheel-independent-drive electric vehicles using optimal torque allocation and dynamic message priority scheduling,” *Control Engineering Practice*, vol. 24, pp. 55 – 66, 2014.
- [24] Y. Chen and J. Wang, “Adaptive energy-efficient control allocation for planar motion control of over-actuated electric ground vehicles,” *IEEE Transactions on Control Systems Technology*, vol. 22, no. 4, pp. 1362–1373, July 2014.
- [25] J. Tjonnas and T. A. Johansen, “Stabilization of Automotive Vehicles Using Active Steering and Adaptive Brake Control Allocation,” *IEEE Transactions on Control Systems Technology*, vol. 18, no. 3, pp. 545–558, may 2010.
- [26] J. Tjonnäs and T. A. Johansen, “Adaptive control allocation,” *Automatica*, vol. 44, no. 11, pp. 2754–2765, nov 2008.
- [27] O. Temiz, M. Cakmakci, and Y. Yildiz, “A Fault Tolerant Vehicle Stability Control Using Adaptive Control Allocation,” in *Dynamic Systems and Control Conference*. ASME, sep 2018, p. V001T09A002.
- [28] —, “Adaptive Control Allocation with Communication Delay for In-Wheel Propulsion Electric Vehicles,” vol. 52, no. 20, Chicago, 2019, pp. 157–162.
- [29] S. P. Software, “Simcenter amesim r13),” 1995. [Online]. Available: <https://www.plm.automation.siemens.com/global/en/products/simcenter/simcenter-amesim.html>
- [30] S. S. Tohidi, Y. Yildiz, and I. Kolmanovsky, “Fault tolerant control for over-actuated systems: An adaptive correction approach,” *Proceedings of the American Control Conference*, vol. 2016-July, pp. 2530–2535, 2016.
- [31] S. Tohidi, Y. Yildiz, and I. Kolmanovsky, “Adaptive control allocation for over-actuated systems with actuator saturation,” *IFAC-PapersOnLine*, vol. 50, no. 1, pp. 5492 – 5497, 2017, 20th IFAC World Congress.
- [32] S. S. Tohidi, Y. Yildiz, and I. Kolmanovsky, “Adaptive control allocation for constrained systems,” *Automatica*, to be published, 2020, Available: <https://drive.google.com/file/d/1gvWlGfwBF27GnW6pmvlweyGnlGwn6L6/view>.
- [33] G. Genta and L. Morello, *The automotive chassis: Components design. Vol. 1*, 1st ed. Springer Netherlands, 2009, vol. 1.
- [34] U. Kiencke and L. Nielsen, *Automotive control systems: For engine, driveline, and vehicle: Second edition*, 2005.
- [35] H. B. Pacejka, *Tire and Vehicle Dynamics*, 2006.
- [36] S. Ikenaga, F. L. Lewis, J. Campos, and L. Davis, “Active suspension control of ground vehicle based on a full-vehicle model,” in *Proceedings of the American Control Conference*, 2000.
- [37] O. Temiz, “Development of control oriented vehicle models and their application to adaptive control allocation problems,” Master’s thesis, Bilkent University, Ankara, 10 2018.
- [38] R. Rajamani, *Vehicle Dynamics and Control*, ser. Mechanical Engineering Series. Springer US, 2011.
- [39] O. Hrkergd and S. T. Glad, “Resolving actuator redundancyoptimal control vs. control allocation,” *Automatica*, vol. 41, no. 1, pp. 137 – 144, 2005.
- [40] O. Hrkergd, “Dynamic control allocation using constrained quadratic programming,” *Journal of Guidance, Control, and Dynamics*, vol. 27, no. 6, pp. 1028–1034, 2004.
- [41] E. Lavretsky and T. E. Gibson, “Projection Operator in Adaptive Systems,” 2011.
- [42] R. Marino, S. Scalzi, and F. Cinili, “Nonlinear PI front and rear steering control in four wheel steering vehicles,” *User Modeling and User-Adapted Interaction*, vol. 45, no. 12, pp. 1149–1168, 2007.
- [43] S. Ikenaga, F. L. Lewis, J. Campos, and L. Davis, “Active suspension control of ground vehicle based on a full-vehicle model,” in *Proceedings of the 2000 American Control Conference. ACC (IEEE Cat. No.00CH36334)*, vol. 6, June 2000, pp. 4019–4024 vol.6.
- [44] S. Skogestad and I. Postlethwaite, *Multivariable Feedback Control: Analysis and Design*. Hoboken, NJ, USA: John Wiley and Sons, Inc., 2005.

VI. APPENDIX

A. Matrices for Control Allocation

$$\mathbf{d}^T = \left[\frac{V_0^2 \rho C_d A}{2} \quad 0 \quad 0 \quad -\frac{V_0^2 \rho C_d A}{2} \quad 0 \right], \quad (56)$$

where V_0 is linearized longitudinal velocity constant.

$$\mathbf{B}_y(t) = \begin{bmatrix} \mathbf{B}_{y1} & \mathbf{B}_{y2} & \mathbf{B}_{y3} & \mathbf{B}_{y4} & \mathbf{B}_{y5} & \mathbf{B}_{y6} \\ \mathbf{B}_{y7} & \mathbf{B}_{y8} & \mathbf{B}_{y9} & \mathbf{B}_{y10} & \mathbf{B}_{y11} & \mathbf{B}_{y12} \end{bmatrix}. \quad (57)$$

where

$$\begin{aligned} \mathbf{B}_{y1} &= [0 \quad C_\alpha N_{fl}(t) \cos(\delta_{fl}) \quad C_\alpha a N_{fl}(t) \cos(\delta_{fl}) \quad 0 \quad 0]^T \\ \mathbf{B}_{y2} &= [0 \quad C_\alpha N_{fr}(t) \cos(\delta_{fr}) \quad C_\alpha a N_{fr}(t) \cos(\delta_{fr}) \quad 0 \quad 0]^T \\ \mathbf{B}_{y3} &= [0 \quad C_\alpha N_{rl}(t) \cos(\delta_{rl}) \quad -C_\alpha b N_{rl}(t) \cos(\delta_{rl}) \quad 0 \quad 0]^T \\ \mathbf{B}_{y4} &= [0 \quad C_\alpha N_{rr}(t) \cos(\delta_{rr}) \quad -C_\alpha b N_{rr}(t) \cos(\delta_{rr}) \quad 0 \quad 0]^T \\ \mathbf{B}_{y5} &= \left[\frac{\cos(\delta_{fl})}{R} \quad 0 \quad \frac{w \cos(\delta_{fl})}{2} \quad 0 \quad 0 \right]^T \\ \mathbf{B}_{y6} &= \left[\frac{\cos(\delta_{fr})}{R} \quad 0 \quad -\frac{w \cos(\delta_{fr})}{2} \quad 0 \quad 0 \right]^T \\ \mathbf{B}_{y7} &= \left[\frac{\cos(\delta_{rl})}{R} \quad 0 \quad \frac{w \cos(\delta_{rl})}{2} \quad 0 \quad 0 \right]^T \\ \mathbf{B}_{y8} &= \left[\frac{\cos(\delta_{rr})}{R} \quad 0 \quad -\frac{w \cos(\delta_{rr})}{2} \quad 0 \quad 0 \right]^T \\ \mathbf{B}_{y9} &= [0 \quad 0 \quad 0 \quad w/2 \quad -a]^T \\ \mathbf{B}_{y10} &= [0 \quad 0 \quad 0 \quad w/2 \quad -a]^T \\ \mathbf{B}_{y11} &= [0 \quad 0 \quad 0 \quad -w/2 \quad b]^T \\ \mathbf{B}_{y12} &= [0 \quad 0 \quad 0 \quad w/2 \quad b]^T, \end{aligned} \quad (58)$$

where C_α is the linearized friction coefficient.

$$\mathbf{B}_n = \text{diag} \left\{ \frac{4N_{fl}}{m} \cos(\delta_{fl}), \frac{N_{fr}}{m} \cos(\delta_{fr}), \frac{4N_{rl}}{m} \cos(\delta_{rl}), \frac{4N_{rr}}{m} \cos(\delta_{rr}), \cos(\delta_{fl}), \cos(\delta_{fr}), \cos(\delta_{rl}), \cos(\delta_{rr}), 1, 1, 1, 1 \right\}. \quad (59)$$

$$\mathbf{B}_l = \begin{bmatrix} \mathbf{B}_{l1} & \mathbf{B}_{l2} & \mathbf{B}_{l3} & \mathbf{B}_{l4} & \mathbf{B}_{l5} & \mathbf{B}_{l6} \\ \mathbf{B}_{l7} & \mathbf{B}_{l8} & \mathbf{B}_{l9} & \mathbf{B}_{l10} & \mathbf{B}_{l11} & \mathbf{B}_{l12} \end{bmatrix}, \quad (60)$$

where

$$\begin{aligned} \mathbf{B}_{l1} &= [0 \quad C_\alpha m/4 \quad a C_\alpha m/4 \quad 0 \quad 0]^T \\ \mathbf{B}_{l2} &= [0 \quad C_\alpha m/4 \quad a C_\alpha m/4 \quad 0 \quad 0]^T \\ \mathbf{B}_{l3} &= [0 \quad C_\alpha m/4 \quad -b C_\alpha m/4 \quad 0 \quad 0]^T \\ \mathbf{B}_{l4} &= [0 \quad C_\alpha m/4 \quad -b C_\alpha m/4 \quad 0 \quad 0]^T \\ \mathbf{B}_{l5} &= [1/R \quad 0 \quad -w/2 \quad 0 \quad 0]^T \\ \mathbf{B}_{l6} &= [1/R \quad 0 \quad w/2 \quad 0 \quad 0]^T \\ \mathbf{B}_{l7} &= [1/R \quad 0 \quad -w/2 \quad 0 \quad 0]^T \\ \mathbf{B}_{l8} &= [1/R \quad 0 \quad w/2 \quad 0 \quad 0]^T \\ \mathbf{B}_{l9} &= [0 \quad 0 \quad 0 \quad w/2 \quad -a]^T \\ \mathbf{B}_{l10} &= [0 \quad 0 \quad 0 \quad -w/2 \quad -a]^T \\ \mathbf{B}_{l11} &= [0 \quad 0 \quad 0 \quad w/2 \quad b]^T \\ \mathbf{B}_{l12} &= [0 \quad 0 \quad 0 \quad -w/2 \quad b]^T. \end{aligned} \quad (61)$$

B. Close Loop Stability

Consider the plant dynamics given in (44). Using (26), the Laplace transform of first element of the virtual control input $\mathbf{V}(s)$ can be written as

$$\mathbf{V}_1(s) = (F_{ref}(s) - F(s))(K_{pf} + K_{if}/s), \quad (62)$$

where, $F(s)$ can be expressed as $F(s) = ma_x(s)$. Similarly, the second element of $\mathbf{V}(s)$ can be written, by using (31), as

$$\mathbf{V}_2(s) = (\beta_{ref}(s) - \beta(s))(K_{py} + K_{iy}/s), \quad (63)$$

where, side-slip angle β can be expressed as $\beta(s) = V_y(s)/V_0$. Using (29), the third element of $\mathbf{V}(s)$ can be obtained as

$$\mathbf{V}_3(s) = (r_{ref}(s) - r(s))(K_{pm} + K_{im}/s) + \beta(s)(K_{ps} + K_{is}/s). \quad (64)$$

Finally, last two elements of $\mathbf{V}(s)$ can be obtained by taking the Laplace transform of (30) as

$$\begin{aligned} \mathbf{V}_4(s) &= (\theta_{ref}(s) - \theta(s))(K_{pp} + K_{ip}/s + sK_{dp}) \\ \mathbf{V}_5(s) &= (\phi_{ref}(s) - \phi(s))(K_{pr} + K_{ir}/s + sK_{dr}). \end{aligned} \quad (65)$$

Using (62) - (65), $\mathbf{V}(s)$ can be expressed in vector form as

$$\mathbf{V}(s) = \begin{bmatrix} (F_{ref}(s) - ma_x(s))(K_{pf} + K_{if}/s) \\ (\beta_{ref}(s) - \frac{V_y(s)}{V_0})(K_{py} + K_{iy}/s) \\ (r_{ref}(s) - r(s))(K_{pm} + K_{im}/s) + \frac{V_y(s)}{V_0}(K_{ps} + K_{is}/s) \\ (\theta_{ref}(s) - \theta(s))(K_{pp} + K_{ip}/s + sK_{dp}) \\ (\phi_{ref}(s) - \phi(s))(K_{pr} + K_{ir}/s + sK_{dr}) \end{bmatrix}, \quad (66)$$

which can be rewritten as

$$\mathbf{V}(s) = \mathbf{K}(s)(\mathbf{R}(s) - \mathbf{Y}(s)), \quad (67)$$

where $\mathbf{R}(s)$ is the Laplace transform of the reference vector,

$$\mathbf{r} = [F_{ref} \quad \beta_{ref} \quad r_{ref} \quad \theta_{ref} \quad \phi_{ref}], \quad (68)$$

$\mathbf{Y}(s)$ is the Laplace transform of the output vector

$$\mathbf{y} = [F \quad \beta \quad r \quad \theta \quad \phi], \quad (69)$$

and $\mathbf{K}(s)$ is the Laplace transform of the control matrix, whose rows are given as

$$\begin{aligned} \mathbf{K}_1(s) &= [(K_{pf} + K_{if}/s) \quad 0 \quad 0 \quad 0 \quad 0] \\ \mathbf{K}_2(s) &= [0 \quad (K_{py} + K_{iy}/s) \quad 0 \quad 0 \quad 0] \\ \mathbf{K}_3(s) &= [0 \quad (K_{pb} + K_{ib}/s) \quad (K_{pmz} + K_{imz}/s) \quad 0 \quad 0] \\ \mathbf{K}_4(s) &= [0 \quad 0 \quad 0 \quad (K_{pmx} + K_{imx}/s + K_{dmx}) \quad 0] \\ \mathbf{K}_5(s) &= [0 \quad 0 \quad 0 \quad 0 \quad (K_{imy} + K_{imy}/s + K_{dmy})]. \end{aligned} \quad (70)$$

Taking the Laplace transformation of (44), we obtain that

$$s\mathbf{X}(s) = \mathbf{A}\mathbf{X}(s) + \mathbf{B}_v\mathbf{V}(s). \quad (71)$$

Furthermore, $\mathbf{Y}(s)$ can be expressed as

$$\mathbf{Y}(s) = \mathbf{C}\mathbf{X}(s) + \mathbf{H}\mathbf{V}(s) \quad (72)$$

where \mathbf{C} and \mathbf{H} are given as

$$\mathbf{C}^T = \begin{bmatrix} V_0 & 0 & 0 & 0 & 0 \\ \rho C_d A & 1/V_0 & 0 & 0 & 0 \\ 0 & 0 & 1 & 0 & 0 \\ 0 & 0 & 0 & 0 & 0 \\ 0 & 0 & 0 & 0 & 0 \\ 0 & 0 & 0 & 1 & 0 \\ 0 & 0 & 0 & 0 & 0 \\ 0 & 0 & 0 & 0 & 1 \\ 0 & 0 & 0 & 0 & 0 \\ 0 & 0 & 0 & 0 & 0 \\ 0 & 0 & 0 & 0 & 0 \\ 0 & 0 & 0 & 0 & 0 \\ 0 & 0 & 0 & 0 & 0 \\ 0 & 0 & 0 & 0 & 0 \\ 0 & 0 & 0 & 0 & 0 \\ 0 & 0 & 0 & 0 & 0 \\ 0 & 0 & 0 & 0 & 0 \end{bmatrix} \quad (73)$$

$$\mathbf{H} = \begin{bmatrix} 1 & 0 & 0 & 0 & 0 \\ 0 & 0 & 0 & 0 & 0 \\ 0 & 0 & 0 & 0 & 0 \\ 0 & 0 & 0 & 0 & 0 \\ 0 & 0 & 0 & 0 & 0 \end{bmatrix}. \quad (74)$$

Using (71) and (72), we obtain that

$$\mathbf{Y}(s) = (\mathbf{C}(s\mathbf{I} - \mathbf{A})^{-1}\mathbf{B}_v + \mathbf{H})\mathbf{V}(s). \quad (75)$$

Defining $\mathbf{G}(s) \equiv \mathbf{C}(s\mathbf{I} - \mathbf{A})^{-1}\mathbf{B}_v + \mathbf{H}$ and substituting (67) into (75), the relationship between the reference signal and the output vector can be written as

$$\mathbf{Y}(s) = (s\mathbf{I} + \mathbf{G}(s)\mathbf{K}(s))^{-1}\mathbf{G}(s)\mathbf{K}(s)\mathbf{R}(s). \quad (76)$$

Considering the definitions,

$$\begin{aligned} \mathbf{T}_0(s) &= (s\mathbf{I} + \mathbf{G}(s)\mathbf{K}(s))^{-1}\mathbf{G}(s), \\ \mathbf{S}_0(s) &= (s\mathbf{I} + \mathbf{G}(s)\mathbf{K}(s))^{-1}, \end{aligned} \quad (77)$$

it can be shown that $\mathbf{T}_0(s)$, $\mathbf{S}_0(s)\mathbf{G}(s)$ and $\mathbf{K}(s)\mathbf{S}_0(s)$ are stable. Therefore the MIMO system, whose dynamics are given by (67) - (75) are internally stable [44].